JOURNAL OF MATERIALS SCIENCE 28 (1993) 5123–5132

# Quantitative determination of the stability of SiC whisker in reaction-bonded/hot-pressed $Si_3N_4$ composites by X-ray diffraction

S. T. J. CHEN, J. -M. YANG
*Department of Materials Science and Engineering, University of California, Los Angeles, CA 90024-1595, USA*

A method was developed for the quantitative determination of weight fractions of the phases in SiC whisker-reinforced reaction-bonded $Si_3N_4$ composites using X-ray diffraction. Composites with different amounts of sintering additives and whiskers were fabricated using reaction bonding followed by hot pressing. The amount of whiskers remaining in each composite after each processing stage was determined. In order to study the degradation mechanism, the microstructural development after each processing step was examined using scanning and transmission electron microscopy. Finally, the effect of sintering additives on the microstructural development and whisker stability was also investigated.

## 1. Introduction

Silicon nitride-based ceramics are one of the most promising classes of structural materials for high-temperature applications [1]. In particular, $Si_3N_4$ has high strength at high temperature, good thermal stress resistance due to the low thermal expansion coefficient, and good oxidation and corrosion resistance. However, the critical factor limiting $Si_3N_4$ in structural applications is its tendency toward catastrophic brittle failure, which reduces its reliability. One approach to substantially improve the fracture toughness, strength and reliability is through the incorporation of second-phase reinforcements [2, 3]. SiC whiskers have been successfully incorporated into $Si_3N_4$ matrix by various processing techniques such as hot pressing, hot isostatic pressing and reaction bonding [4–11]. It is expected that the composite approach would greatly improve the strength, toughness and reliability of the monolithic $Si_3N_4$. However, only some limited success in developing SiC whisker-reinforced $Si_3N_4$ with improved strength and toughness has been reported. Most of the works resulted in lower strength and toughness for the composites than for the monolithic $Si_3N_4$. The reduction of mechanical properties is attributed mainly to the processing flaws such as porosity, whisker agglomeration and whisker degradation [2, 4, 8, 10, 11]. A previous study indicated that SiC whiskers served as growth sites for $Si_3N_4$ during reaction bonding [12]. Substantial degradation of SiC whiskers in an $Si_3N_4$ matrix also occurred during sintering and hot isostatic pressing [12]. The degradation of the SiC whiskers was mainly attributed to surface impurities. The sintering additives used to promote liquid phase may also affect the stability of the SiC whiskers [12]. The degradation of the SiC whiskers would ultimately affect the strength and toughness of the resulting composite. Up to now, very little work has been conducted to quantify the amount of whiskers remaining in the composite after each processing stage. Quantitative analysis of phase content in a composite using X-ray diffraction (XRD) is often very difficult because many variables such as structure factors, absorption coefficients, particle size, and identification and resolution of diffraction peaks for each phase contained have to be considered in order to accurately determine the relative amounts of each phase.

The purpose of this work was to establish a reliable technique to determine the stability of SiC whiskers in an $Si_3N_4$ matrix and to study the mechanism of whisker degradation by quantitative X-ray analysis. Particular emphasis was placed on determining the extent of whisker degradation after each processing stage.

## 2. Experimental procedure

### 2.1. Materials and processing

Commercial SiC whiskers produced by American Matrix (Knoxville, Tennessee) were used as reinforcement. X-ray diffraction (XRD) analysis showed that the whiskers contained 100% β-SiC phase. $Al_2O_3$ and $Y_2O_3$ powders were introduced before the nitridation stage as sintering additives. Different amounts of the sintering additives were employed to develop three types of $Si_3N_4$ matrix compositions, as listed in Table I. For Type I and Type II composites, the ratio of $Y_2O_3$ to $Al_2O_3$ was the same. However, the amount of sintering additives in Type I composites was four times that of Type II composites. Type III composites contained the highest total amount of sintering

0022–2461 

TABLE I The matrix compositions in different systems

| Matrix system | Relative content (wt %) | | |
|---|---|---|---|
| | $Si_3N_4$ | $Y_2O_3$ | $Al_2O_3$ |
| Type I | 91 | 8 | 1 |
| Type II | 97.75 | 2 | 0.25 |
| Type III | 83 | 6 | 11 |

additives among all. The procedures for fabricating these composites were as follows.

The Si powders (Kema Nord Industrukemi, Sweden), with mean particle size of 4 μm, along with $Y_2O_3$ and $Al_2O_3$ powder (1 μm) were first dry-milled. The SiC whiskers were then introduced into the slurry and dispersed through wet milling in isopropyl alcohol. The slurry was then dried, dry-milled and screened. The resulting powder mixture was cold-formed into 15 cm by 15 cm plates, with a thickness of 3 cm, using die pressing under 10 MPa at room temperature. The powder compacts were nitrided in a cold-wall, refractory metal furnace controlled by a nitrogen demand system operating from 1100 to 1400 °C for about 192 h. A microprocessor was used to keep the nitrogen partial pressure at 0.75 atm. To assist the nitridation of silicon, the temperature was programmed according to the nitrogen consumption rate.

The nitrided preforms were then densified using hot pressing under a pressure of 25 MPa at 1780 °C for 2 h in an $N_2$ atmosphere (0.8 atm). Before the composites were taken out of hot pressing, an annealing was performed by releasing the pressure at 1200 to 1400 °C for 1 to 2 h to reduce the residual stress in the composites. Composites with 10, 20, 30, and 40 vol% of SiC whiskers were produced. Both scanning electron microscopy (SEM) and transmission electron microscopy (TEM) were used to characterize the microstructure of the composite after each processing stage.

### 2.2. XRD quantitative analysis

The specimens for X-ray diffraction analysis were prepared from Type I, Type II, and Type III composites. Standard samples for generating the X-ray calibration curve were also prepared by mixing the silicon nitride powders with 10, 20, 30 and 40 vol% of SiC whiskers. All specimens were ground to fine powder form (~300 mesh). Specimens were run in standard specimen holders on a diffractometer using monochromatic Cu$K_\alpha$ radiation. The scanning rate was 0.005 °(2θ) $s^{-1}$ and the counting time was 3 s in order to obtain enough intensity to measure.

Although existing crystal structure data are sufficient for indexing powder patterns, they are generally inadequate for use in developing a procedure for quantitative analysis. Therefore, a computer simulation program was developed to generate the XRD pattern and the peak intensity which were based on the best atomic parameters available. The procedures adopted for quantitative XRD analysis are briefly described below. A detailed description of the XRD quantitative analysis is given in Gazzara and Messier [13]. For XRD quantitative analysis, preferred orientation is one of the problems that cannot be avoided in a specimen containing different grain morphologies [14]. As a result, a normalizing factor is necessary to correct the measured peaks for the phase having such a problem. In order to do that, several peak intensities simulated from computer program and those measured from XRD experiments for each phase in a specimen were compared and analysed to obtain a normalizing factor. This factor was then used to correct each measured peak intensity for that phase. Finally, the corrected peak intensity of each phase was used to calculate the amount of each phase in a specimen.

The atomic parameters needed for computer-generated XRD intensity powder data for α- and β-$Si_3N_4$, β-SiC, $YSiO_2N$ (K phase) and $Y_{10}N_2Si_6O_{24}$ (H phase) were obtained from the literature [15–18]. To minimize the effects of preferred orientation and particle size, selected peaks of each phase should be as many as possible and should have good resolution, freedom from overlap and sufficient intensity to ensure statistical precision [13]. Therefore, the peaks selected for phase α-$Si_3N_4$ were (1 0 1), (1 1 0), (2 0 0), (2 0 1), (1 0 2), (2 1 0) and (3 0 1). The peaks for phase β-$Si_3N_4$ were (1 1 0), (2 0 0), (1 0 1) and (2 0 1). The peaks for phase β-SiC were (1 1 1), (2 2 0) and (3 1 1). The peaks for phase $YSiO_2N$ (K phase) were (0 0 2), (1 1 0), (1 1 2) and (3 0 0). Peak (2 1 1) was selected for the $Y_{10}N_2Si_6O_{24}$ (H phase).

## 3. Results

### 3.1. Simulated and measured XRD patterns

The computer-generated XRD patterns for α-$Si_3N_4$, β-$Si_3N_4$, β-SiC, $YSiO_2$ (K phase) and $Y_{10}N_2Si_6O_{24}$ (H phase) are shown in Figs 1–5, respectively. The 2θ positions and the *R* factors for those selected peaks in each phase are also listed in Table II. The (*hkl*) indices of the strongest peaks in each phase simulated from the computer program were (2 1 0) for α-$Si_3N_4$, (1 0 1) for β-$Si_3N_4$, (1 1 1) for β-SiC, (1 1 2) for K phase and (2 1 1) for H phase. The corresponding values of *R* factor were 9.099, 11.785, 38.566, 58.969 and 64.407, respectively. All these patterns were very consistent with those obtained from the Standard JCPDS Card File. It was found that the *R* factor for peak (2 2 1) in the H phase and peak (1 1 2) in the K phase are approximately five times higher than that of the strongest peak in α- or β-$Si_3N_4$. The *R* factor of the peak (1 1 1) in β-SiC was three to four times higher than that of the strongest peak in α- or β-$Si_3N_4$.

### 3.2. Standard calibration curve

The equations used to calculate the phase content were based on the perfectly random mixing condition. Due to the difference in particle sizes between $Si_3N_4$ grains and SiC whiskers and the effects of preferred orientation and extinction, a standard calibration curve has to be established in order to relate the

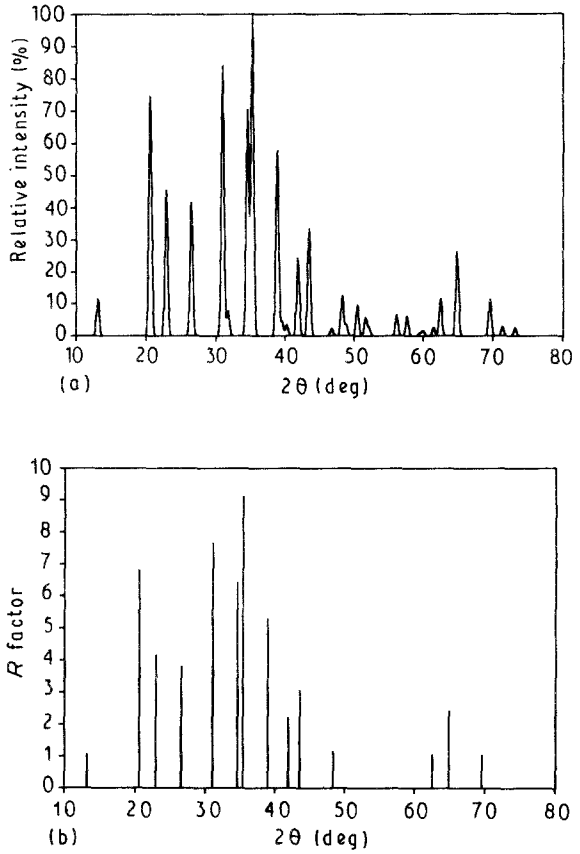


*Figure 1* Computer-simulated (a) XRD pattern, (b) XRD *R* factor for $\alpha$-$Si_3N_4$.

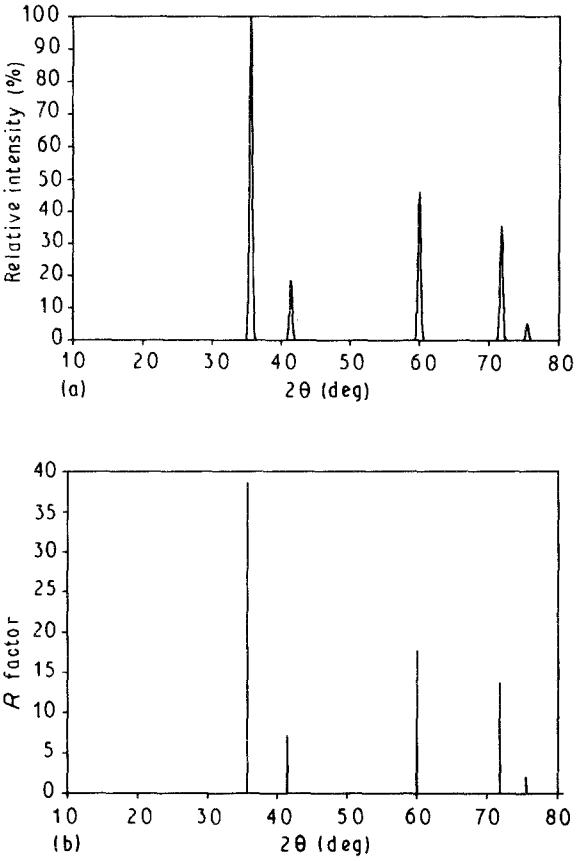


*Figure 3* Computer-simulated (a) XRD pattern, (b) XRD *R* factor for $\beta$-SiC.

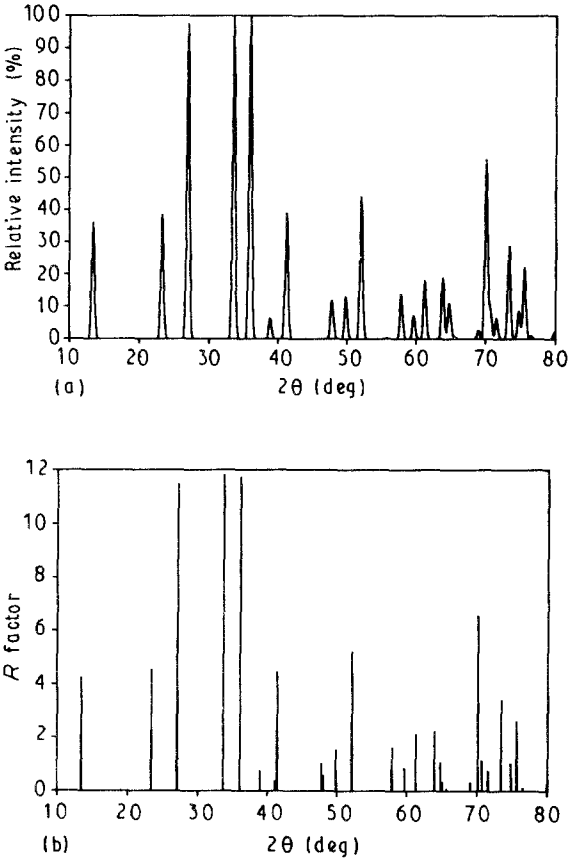


*Figure 2* Computer-simulated (a) XRD pattern, (b) XRD *R* factor for $\beta$-$Si_3N_4$.

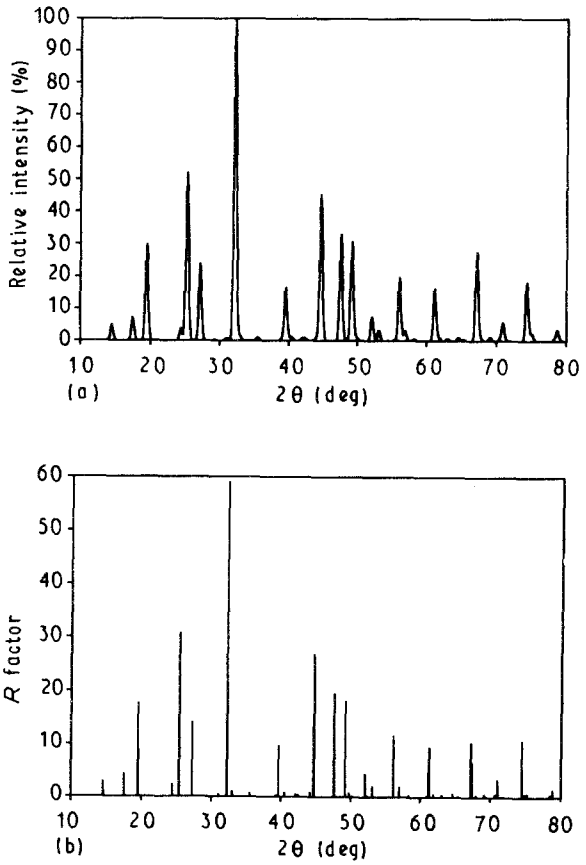


*Figure 4* Computer-simulated (a) XRD pattern, (b) XRD *R* factor for K phase.

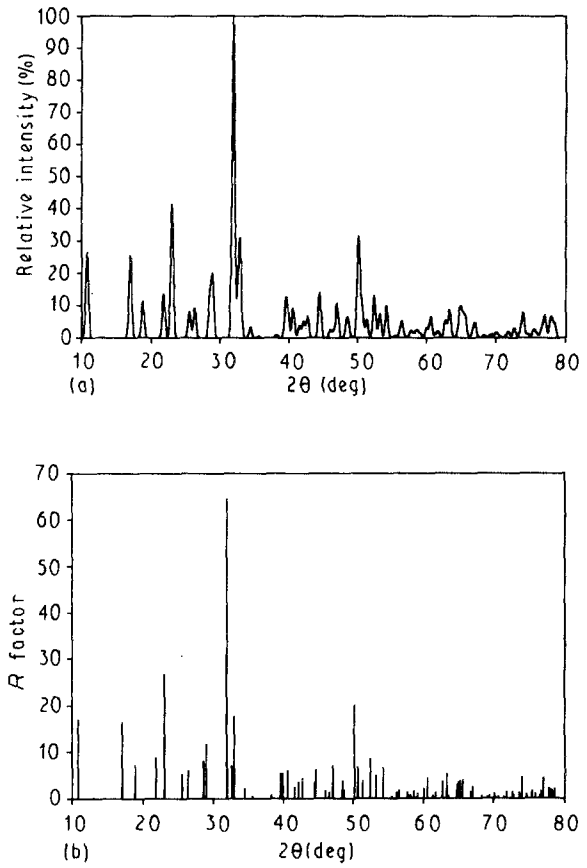


*Figure 5* Computer-simulated (a) XRD pattern, (b) XRD *R* factor for H phase.

TABLE II The 2θ positions and corresponding *R* factor of selected peaks for each phase

| Phase | Peak | 2θ | *R* factor |
|---|---|---|---|
| α-$Si_3N_4$ | (1 0 1) | 20.61 | 6.792 |
| | (1 1 0) | 22.94 | 4.142 |
| | (2 0 0) | 26.55 | 3.792 |
| | (2 0 1) | 31.03 | 7.655 |
| | (1 0 2) | 34.60 | 6.397 |
| | (2 1 0) | 35.37 | 9.099 |
| | (3 0 1) | 43.52 | 3.065 |
| β-$Si_3N_4$ | (1 1 0) | 23.38 | 4.531 |
| | (2 0 0) | 27.06 | 11.453 |
| | (1 0 1) | 33.65 | 11.785 |
| | (2 0 1) | 41.39 | 4.451 |
| β-SiC | (1 1 1) | 35.68 | 38.566 |
| | (2 2 0) | 60.04 | 17.739 |
| | (3 1 1) | 71.84 | 13.649 |
| $YSiO_2$ (K Phase) | (0 0 2) | 19.50 | 17.568 |
| | (1 1 0) | 25.37 | 30.687 |
| | (1 1 2) | 32.20 | 58.969 |
| | (3 0 0) | 44.71 | 26.747 |
| $Y_{10}N_2Si_6O_{24}$ (H phase) | (2 1 1) | 31.92 | 64.407 |

amount of SiC whiskers measured in a composite specimen after nitridation and nitridation/hot-pressing to that of the SiC whiskers in the powder mixture prior to processing. The standard calibration curve would then ensure the analysed data to be reliable and reproducible.

As shown in Fig. 6, the plot of $x/(1-x)$ versus $x$ gives the standard calibration curve, where $x$ represents the amount of the SiC whiskers. The ratio $x/(1-x)$ obtained from a composite was then referred to the standard calibration curve to obtain the actual amount of the SiC whiskers that remained in that composite. The results obtained showed that the accuracy of the XRD quantitative method was 91.5, 86.6, 82.2 and 81.8% for specimens containing 10, 20, 30 and 40 vol % SiC whiskers, respectively. This indicated that the accuracy of the XRD quantitative analysis decreases as the content of the SiC whiskers increases. This may be due to the fact that SiC whiskers have a very long aspect ratio (~20 to ~100). As a result, the approach to perfect random mixing condition in a composite would become worse as the SiC whiskers content increased.

### 3.3. Analysis of phase content and degradation of SiC whiskers

The crystalline second phase after nitridation in Type I composites was found to be K phase. After hot pressing, K phase transformed to H phase. However, the K phase in Type I monolithic matrix remained unchanged after hot pressing. For Type II composites, the crystalline second phase was found to be the same as that in Type I composites. In Type III composites, $3Y_2O_3 \cdot 5Al_2O_3$ (YAG phase) was found to be the crystalline second phase after both nitridation and hot pressing. The relative amount of the K phase for Type I composites was around 5 and 4 wt % after nitridation and hot pressing, respectively. For Type II composites, only a trace amount of K phase was detected. The relative amount of the YAG phase in the Type III composite cannot be determined due to the lack of accurate atomic parameters for the YAG phase unit cell. However, based upon the amount of sintering additives used and the mole ratio of $Y_2O_3$ to $Al_2O_3$ in the YAG phase, the amount of the YAG phase should be less than 17 wt %. Also, the amount of residual glassy phase could not be determined due to the uncertain chemical composition of the glassy phase. However, if the amount of the residual glassy phase were counted, the relative percentage of each phase would be lower.

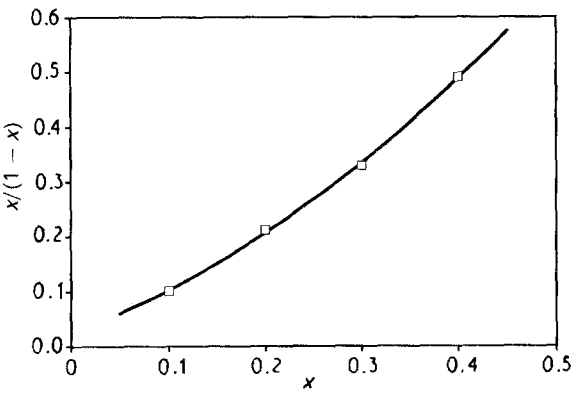


*Figure 6* Calibration curve for the content of SiC whiskers ($x$) in standard specimens.

Fig. 7 shows the degradation of SiC whiskers after nitridation and after nitridation/hot-pressing for each type of composite. Using the linear regression method, the degradation of the SiC whiskers after nitridation is around 27% and 5% for Type I and Type II composites, respectively. For Type III composites, the degradation range of the SiC whiskers was calculated to be in the range of 22 to 36%, assuming the amount of YAG phase was between 0 and 17 wt %. It was also found that the amounts of the SiC whiskers measured after nitridation and hot pressing were about the same. This indicated that the degradation of SiC whiskers occurred primarily during the nitridation stage.

The ratios of β- to α-$Si_3N_4$ after nitridation in these three types of composite are listed in Table III. For both Type I and Type II composites the ratio was around 1/5, while for Type III composites the ratio rose to 2/1. This indicates that the degree of transformation of α- to β-$Si_3N_4$ in Type III composites is around 10 times higher than that in both Type I and Type II composites. After hot pressing, α-$Si_3N_4$ grains were transformed completely to β grains.

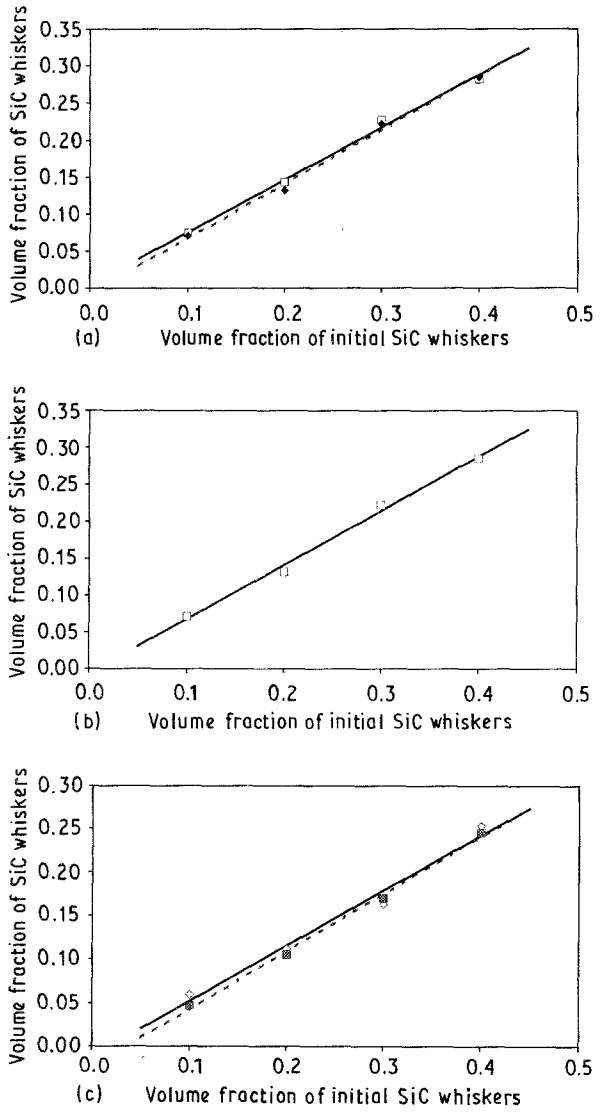


*Figure 7* Experimental results and linear regression lines for different composites, assuming 17 wt % YAG phase. (a) Type I: (◆, ---) reaction-bonded; (□, —) reaction-bonded/hot-pressed. (b) Type II: (□, —) reaction-bonded. (c) Type III: (▩, ---) reaction-bonded; (◇, —) reaction-bonded/hot-pressed.

TABLE III The β-$Si_3N_4$/α-$Si_3N_4$ ratio for Type I, Type II, and Type III composites

| Composite | β-/α-$Si_3N_4$ ratio | | | | |
|---|---|---|---|---|---|
| | 10 vol % | 20 vol % | 30 vol % | 40 vol % | Average |
| Type I | 0.20 | 0.23 | 0.20 | 0.30 | 0.23 |
| Type II | 0.18 | 0.21 | 0.21 | 0.20 | 0.20 |
| Type III | 2.10 | 1.05 | 2.24 | 2.06 | 1.86 |

## 3.4. Microstructural analysis

As shown in Fig. 8, the whisker has a straight, rod-like shape. The diameter was measured to be 2 to 5 μm, and the aspect ratio ranged from 20 to 100. Typical fracture morphologies of the Type I composites containing 10, 20, 30 and 40 vol % SiC whiskers after nitridation are shown in Fig. 9. The fracture morphologies for all compositions of the Type II and Type III composites are similar. Figs 10 and 11 show the typical morphologies for Type II and Type III composites, respectively. As shown in Fig. 9e, needle-like and hump-like materials were located randomly on the surface of the SiC whiskers. Similar morphology was also observed in all types of composite. From the results of Evans and Sharp [19] and Danforth and Richman [20], these needle-like materials are α-$Si_3N_4$ whiskers which are formed through a vapour–liquid–solid mechanism [21]. The needle-like α-$Si_3N_4$ whiskers were frequently found at large microvoids. However, at some small microvoids, these needle-like α-$Si_3N_4$ whiskers were also observed to be merging into the surrounding matrix. For all Type II and Type III composite specimens, some degree of pre-sintering occurred and the grain size of the $Si_3N_4$ matrix was large (~10 μm), as shown in Figs 10 and 11. For Type I composites, only the specimen containing 40 vol % SiC whiskers was observed to have the same pre-sintering morphology and grain size as in the Type II and Type III composites. For the remaining Type I composites, pre-sintering morphology was not observed and the grain size of the $Si_3N_4$ matrix was very small (~1 μm). After hot pressing, a typical microstructure of Type I composites containing 40 vol % SiC whiskers is as shown in Fig. 12. Three different grain geometries cross-linked together were observed: coarser rod-like β-SiC whiskers, and equiaxed and rod-like β-$Si_3N_4$ grains.

A TEM micrograph of the initial SiC whiskers is shown in Fig. 13. Typical stacking faults and the node structure of the SiC whiskers were observed. However, the TEM micrograph of the SiC whisker in Type I composites containing 40 vol % SiC whisker after nitridation indicated that the surface of the SiC whiskers was covered by a thin amorphous layer and that a nucleation site of α-$Si_3N_4$ was found on top of the amorphous layer, as shown in Fig. 14. The growth of needle-like α-$Si_3N_4$ was also observed in Type I composites containing 10 vol % SiC whisker, as shown in

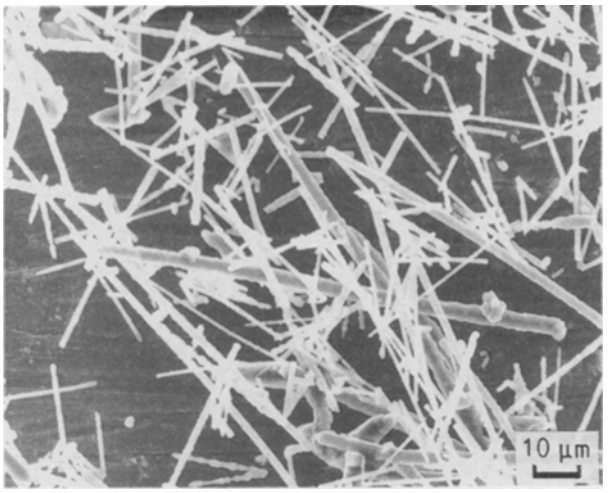


*Figure 8* The SEM morphology of SiC whiskers.

Fig. 15. Similar morphologies were also observed for all compositions in both Type II and Type III composites.

## 4. Discussion

### 4.1. Degradation mechanism of SiC whiskers

The XRD quantitative analysis clearly showed that severe whisker degradation occurred after nitridation. The possible degradation reaction is the nitridation of the SiC whisker to form $Si_3N_4$:

$$3SiC + 2N_2 = Si_3N_4 + 3C$$

Thermodynamic calculations showed that the SiC whisker would suffer degradation under the current nitridation conditions [22, 23]. A previous study also indicated that the SiC whisker degradation reaction given by the above equation could be affected by other

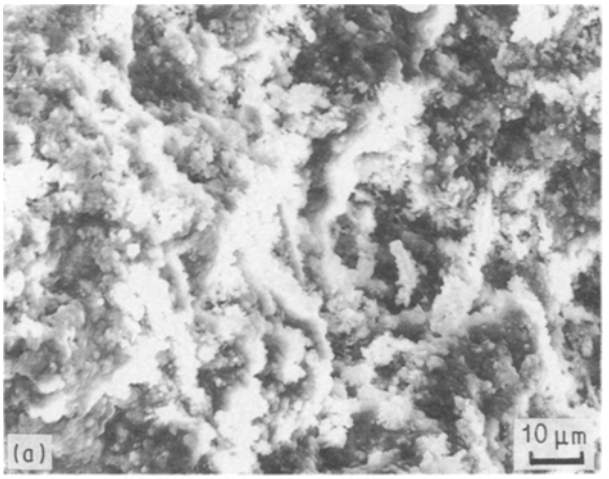


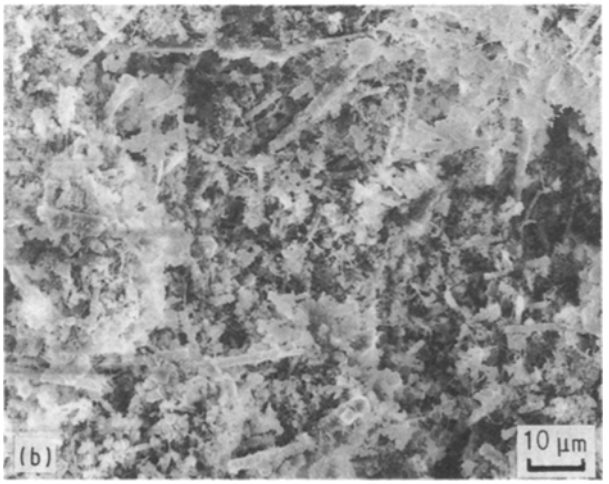


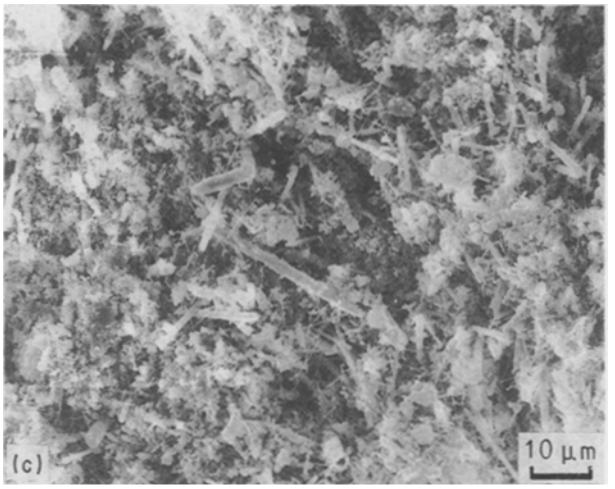


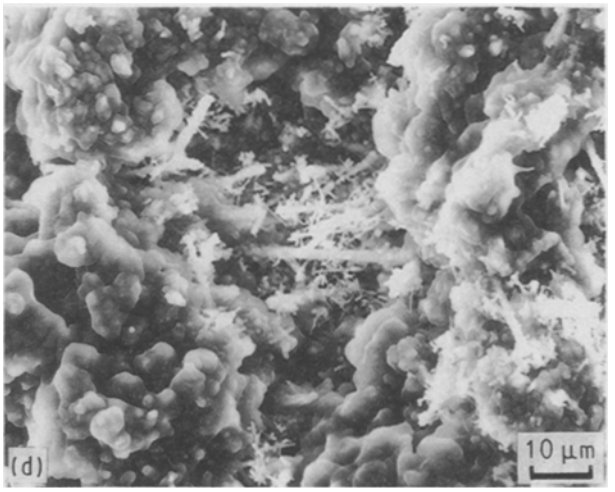


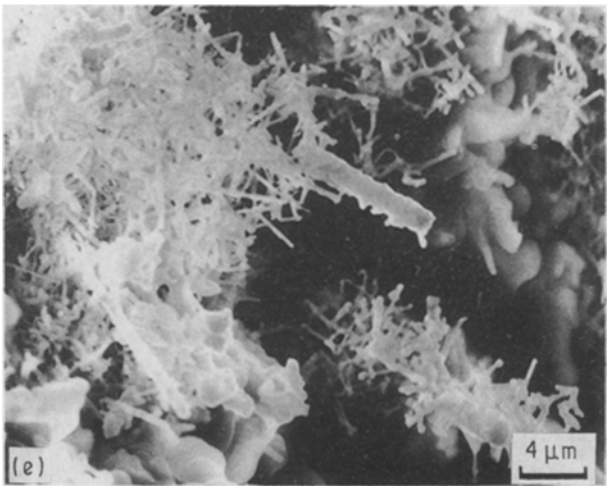


*Figure 9* The SEM morphology of Type I composites containing (a) 10 vol %, (b) 20 vol %, (c) 30 vol %, (d, e) 40 vol % SiC whiskers after nitridation.

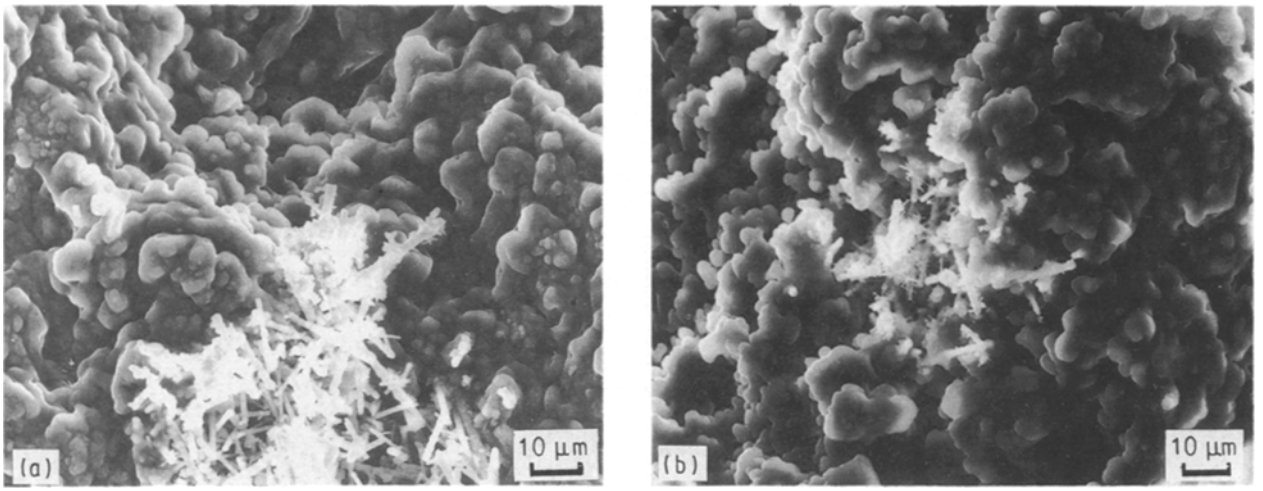


*Figure 10* SEM morphology of Type II composites containing (a) 10 vol %, (b) 20 vol % SiC whiskers after nitridation.

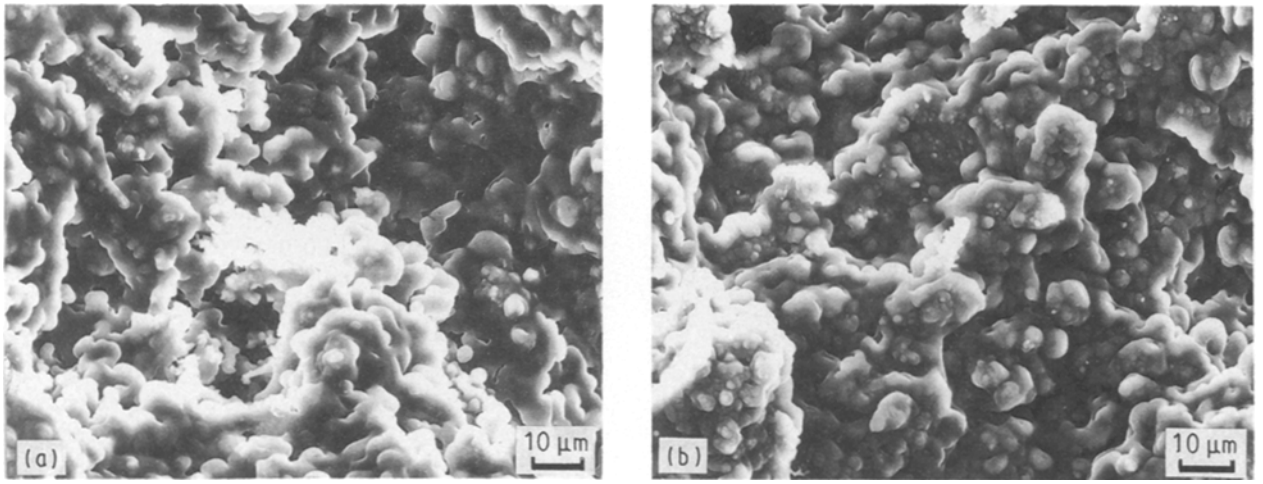


*Figure 11* SEM morphology of Type III composites containing (a) 10 vol %, (b) 20 vol % SiC whiskers after nitridation.

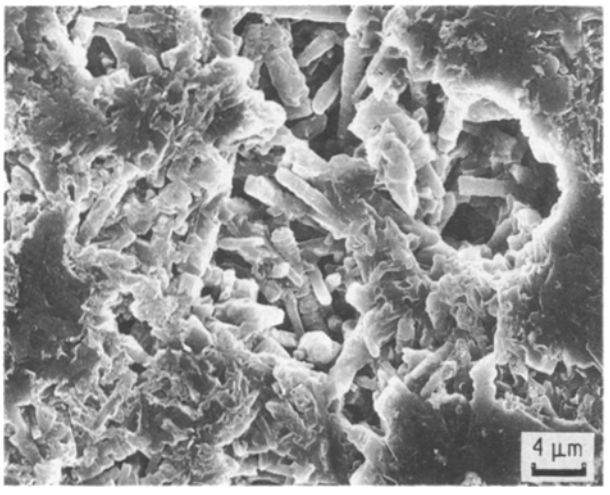


*Figure 12* SEM morphology of Type I composites containing 40 vol % SiC whiskers after nitridation/hot-pressing.

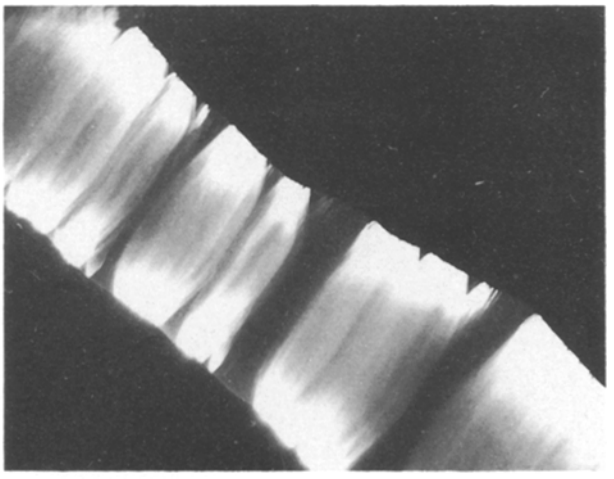

*Figure 13* TEM morphology of SiC whiskers.

factors [12]. For example, the existence of oxygen in a nitrogen atmosphere will favour the degradation of SiC whiskers to proceed by converting the elemental carbon into CO. In addition, impurities on the surface of the SiC whisker such as iron might act as a catalyst to speed up the dissociation of SiC into silicon and carbon. The silicon dissociated from the SiC whisker can oxidize to form SiO or $SiO_2$. Both reactions would promote the consumption of SiC and lead to the degradation of SiC whiskers.

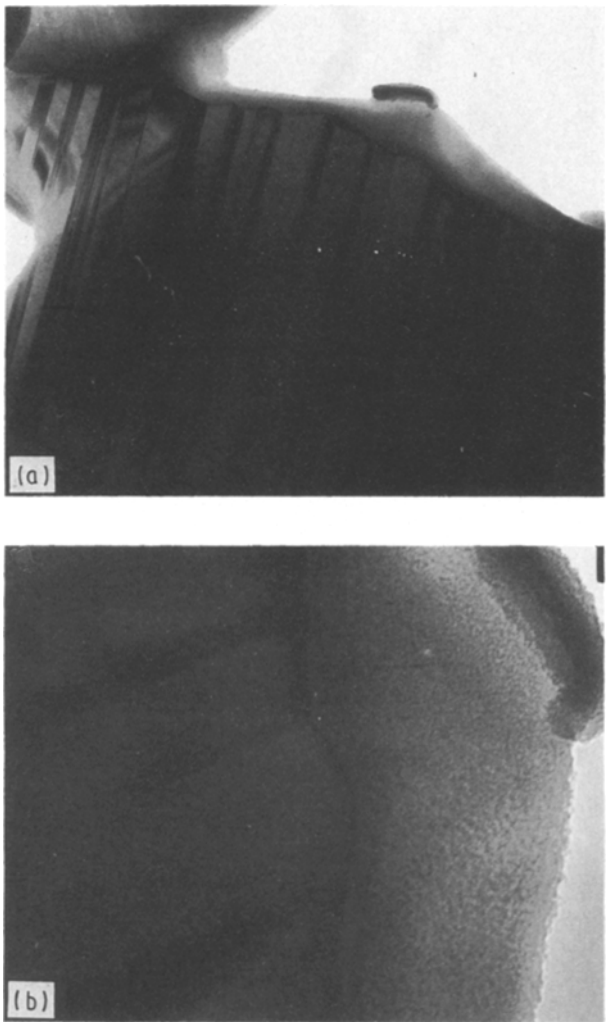


*Figure 14* (a, b) TEM morphology of Type I composites containing 40 vol % SiC whiskers after nitridation, showing the nucleation of $\alpha$-$Si_3N_4$ needles.

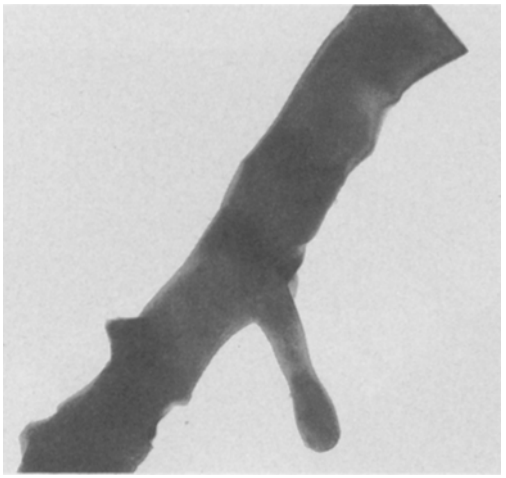

*Figure 15* TEM morphology of Type I composites containing 10 vol % SiC whiskers after nitridation, indicating the growth of $\alpha$-$Si_3N_4$ needles.

Based upon the microstructural observations the possible degradation processes of the SiC whiskers can be deduced as follows:

(a) Initially, nucleation of $\alpha$-$Si_3N_4$ on the SiC whisker surface occurs. As suggested by Boyer and Moulson [24], the surface impurities, especially iron, will catalyse the nitridation of the SiC whisker by devitrifying and/or removing the oxide layer covering the SiC whisker surface. This would result in the direct exposure of the underlying SiC whisker to the nitrogen environment. Therefore, at certain local spots on the surface of the SiC whiskers, supersaturation of $\alpha$-$Si_3N_4$ will be reached and a spherical origin will be formed [19, 20]. This whisker origin acts as a nucleation site for the growth of the $\alpha$-$Si_3N_4$ needles.

(b) Secondly, the growth of $\alpha$-$Si_3N_4$ needles occurs either by the transportation of nitrogen into the whisker origin where it condenses in the liquid and reacts at the solid–liquid interface to form silicon nitride, or by the deposition of $\alpha$-$Si_3N_4$ from the nitridation of the silicon powder on the nucleation sites.

This degradation process is verified by the presence of the randomly orientated tiny, rod-like $\alpha$-$Si_3N_4$ grains grown from the surface of the SiC whiskers. As observed in Figs 9–11, it was found that nitridation of the SiC whiskers always occurred locally at the large pores which can be regarded as a reaction chamber. Nitrogen gas can diffuse into this chamber to react with silicon vapour to form $\alpha$-$Si_3N_4$ which is then deposited on to the nucleation sites. Oxygen can also diffuse in to react with elemental carbon to form CO and/or $CO_2$, which will promote the nitridation reaction of SiC whiskers.

After hot-pressing, minor further degradation of SiC whiskers was found. This can be explained by the fact that the nitrogen source, which promotes the degradation of SiC whiskers, was cut off because the open pores and interconnected microvoids generated during nitridation were closed during hot pressing. The diffusion of nitrogen into the material was difficult and/or the diffusion paths became much longer.

## 4.2. Effect of sintering additives on microstructural development and whisker stability

The results obtained indicate that the extent of whisker degradation and microstructural development among the three types of composite are different. This may be due to the difference in the amounts of sintering additives, which in turn will affect the amount and viscosity of the liquid phases during processing. The phase diagram for the $SiO_2$–$Y_2O_3$–$Al_2O_3$ ternary system is shown in Fig. 16 [25]. Based upon the ratio of $Y_2O_3$ to $Al_2O_3$, the possible locations of the eutectic temperature would lie on line A for both Type I and Type II composites and line B for Type III composites. This indicates that the possible eutectic temperatures for both Type I and Type II composites could be in the range from 1345 to 1740 °C, depending on the amount of $SiO_2$ relative to the total amounts of $Y_2O_3$ and $Al_2O_3$. For Type III composites, the possible eutectic temperatures will be independent of the $SiO_2$ content, always being lower than 1400 °C. A possible source of $SiO_2$ may be from the surfaces of the SiC whiskers and silicon powders. As a result, the $SiO_2$ content and, hence, the eutectic temperature will vary as the composition of the com-

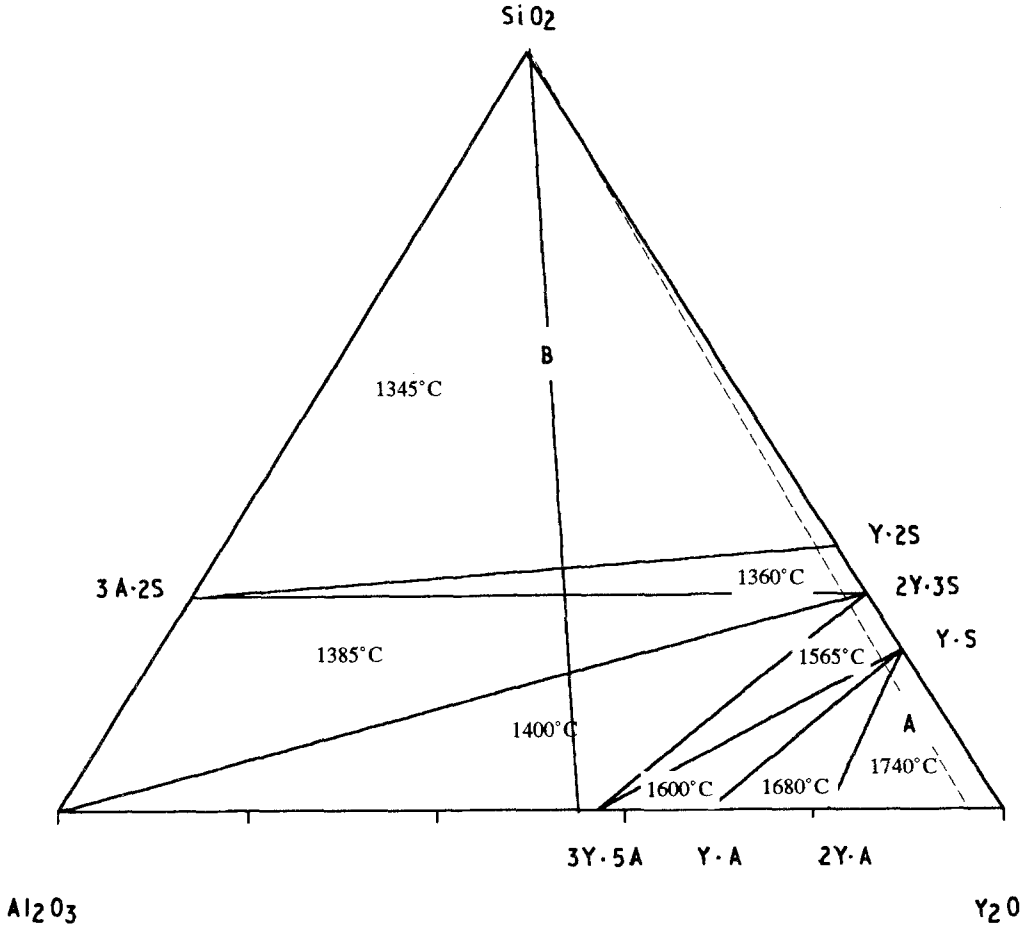


*Figure 16* Phase relations and liquidus temperature in the $Y_2O_3$–$Al_2O_3$–$SiO_2$ ternary system. Line A and Line B are the locations of the possible eutectic temperatures for Type I, Type II and Type III composites, respectively. The unit in the phase diagram is weight per cent.

posite changes. If impurities were involved in the $SiO_2$–$Y_2O_3$–$Al_2O_3$ ternary system, the eutectic temperature would be lower [1]. Under the current nitridation temperatures, most of the sintering additives of Type III composites will react with $SiO_2$ to form a liquid phase. Therefore, the amount of liquid phase formed in Type III composites will be high. However, for both Type I and Type II composites, only local areas where the content of $SiO_2$ is high will have the capability to form a liquid phase. The liquid phase formed during nitridation acted as the medium through which the transformation of α- to β-$Si_3N_4$ could proceed by a solution–diffusion–precipitation mechanism. As shown in Table III, Type III composites have a β- to α-$Si_3N_4$ ratio of 2, which is five times higher than that in both Type I and Type II composites. This indicates that the amount of liquid phase in Type III composites was much higher than that in both Type I and Type II composites during nitridation.

The morphologies in Figs 10 and 11 show that pre-sintering behaviour occurred in all compositions of the Type II and Type III composites. Only the 40 vol % of SiC whiskers in the Type I composite exhibited such a pre-sintering phenomenon. For Type II composites, the pre-sintering morphology could be explained by the small amount of sintering additives relative to the $SiO_2$ content which reduced the eutectic temperature. As a result, most of the sintering additives could be melted and the viscosity of the liquid phase became low. The total amounts of sintering additives in Type I composites are four times higher than in Type II composites. Therefore, higher eutectic temperatures are expected. The fact that pre-sintering was observed only in Type I composites containing 40 vol % SiC whiskers indicated that its eutectic temperature was lower than those of other compositions in Type I composites. Hence, the amount of liquid phase was higher for 40 vol % than for other compositions in Type I composite. This can also be confirmed by the higher β- to α-$Si_3N_4$ ratio in the 40 vol % composite.

Based upon the degradation mechanism of the SiC whiskers during nitridation, the nitridation of the SiC whiskers can be more favourable if the reaction product, $Si_3N_4$, is consumed by being involved in other reactions or by being dissolved into the surrounding matrix. As mentioned previously, the crystalline second phase was K phase for both Type I and Type II composites and YAG phase for Type III composites. The formula for K phase, $2Y_2O_3 \cdot Si_3N_4 \cdot SiO_2$, indicates that $Si_3N_4$ was involved in forming the K phase. The amount of K phase in Type II composites was only a trace. This can explain why only 5% degradation of the SiC whiskers occurred in Type II composites. Compared with Type II composite, 27% degradation of the SiC whiskers occurred in Type I composites in which the amount of K phase was

around 4 wt %. For Type III composites, the formula for YAG phase is $3Y_2O_3 \cdot 5Al_2O_3$, indicating that $Si_3N_4$ was not involved in forming YAG phase; however, the large amount of liquid phase and its low viscosity could dissolve some of the $\alpha$-$Si_3N_4$ grown on the surface of the SiC whiskers. This could promote further degradation of the SiC whiskers in the Type III composites.

## 5. Summary and concluding remarks

1. The XRD quantitative analysis developed here is a rapid and accurate method to determine the phases in SiC whisker reinforced reaction-bonded/hot-pressed $Si_3N_4$ composites. The accuracy of the XRD quantitative method was 91.5, 86.6, 82.2, and 81.8% for the standard specimen of known compositions of 10, 20, 30 and 40 vol % SiC whiskers. This procedure may be useful for analysing phases of other ceramic mixtures.

2. The degradation of SiC whiskers is affected by surface impurities on the SiC whiskers, the amount of initial sintering additives, and the crystalline second phase formed in the matrix during nitridation. Most of the degradation of SiC whiskers was found to occur during nitridation.

3. The degradation process can be described as follows: (i) nucleation of $\alpha$-$Si_3N_4$ occurs initially at certain local spots on the surface of the SiC whiskers, the supersaturation of $\alpha$-$Si_3N_4$ is reached and a spherical origin formed at those spots; and (ii) the growth of the $\alpha$-$Si_3N_4$ needles proceeds either by the transport of nitrogen into the whisker origin to form silicon nitride or by the deposition of $\alpha$-$Si_3N_4$ from nitridation of the silicon powder on the nucleation sites.

## Acknowledgements

This work was partially supported by the National Science Foundation through the Presidential Young Investigator Award to J.-M. Yang (MSS-9057030). The authors also thank Mr A. Ezis at Cercom Inc. for providing the composite materials and Mr Tu-Hoan Bruce Nguyen for reviewing the manuscript.

## References

1. G. ZIEGLER, J. HEINRICH and G. WOTTING, *J. Mater. Sci.* **22** (1987) 3041.
2. P. F. BECHER and T. N. TIEGS, in "Engineering Materials Handbook", Vol. 1, "Composites", (ASM, 1987) p. 941.
3. A. G. EVANS, *Phil. Mag.* **26** (1972) 1327.
4. P. D. SHALEK, J. J. PETROVIC, G. F. HURLEY and F. D. GAC, *Amer. Ceram. Soc. Bull.* **65** (1986) 351.
5. A. BELLOSI and G. DEPORTU, *Mater. Sci. Engng.* **A109** (1989) 357.
6. G. C. WEI and P. F. BECKER, *Amer. Ceram. Soc. Bull.* **64** (1985) 298.
7. S. C. FARMER, P. PIROUZ and A. H. HEUER, *Mater. Res. Soc. Symp. Proc.* **120** (1989) 169.
8. R. HAYAMI, K. UENO, N. TAMARI and Y. TOIBANA, in "Tailoring Multiphase and Composite Ceramics", edited by R. Tressler and G. Messing (Plenum, 1986) p. 663.
9. J. P. SINGH, K. C. GORETTA, D. S. KUPPERMAN and J. L. ROUBORT, *Adv. Ceram. Mater.* **3** (1988) 357.
10. J. S. HAGGERTY, *Mater. Sci. Engng.* **A107** (1989) 117.
11. S. T. BULJAN, J. G. BALDONI, and M. L. HUCKABEE, *Ceram. Bull.* **66** (1987) 347.
12. S. T. BRADLEY and K. R. KARASEK, *J. Amer. Ceram. Soc.* **72** (1989) 628.
13. C. H. GAZZARA and D. R. MESSIER, *Amer. Ceram. Soc. Bull.* **56** (1977) 777.
14. B. D. CULLITY, "Elements of X-Ray Diffraction", 2nd Edn (Addison-Wesley, 1978) p. 140.
15. S. WILD, P. GRIEVESON and K. H. JACK, in "Special Ceramics 5", No. 28 (1970) p. 385.
16. H. THIBAULT, *Amer. Min.* **29** (1944).
17. P. E. D. MORGAN, P. J. CARROLL and F. F. LANGE, *Mater. Res. Bull.* **12** (1977) 251.
18. A. W. J. M. RAE, D. P. THOMPSON, N. J. PIPKIN and K.H. JACK, in "Special Ceramics 6", edited by P. Popper (British Ceramic Research Association, Stoke-on-Trent, UK, 1975) p. 347.
19. A. G. EVANS and J. V. SHARP, in "Electron Microscopy and Structure of Materials," edited by G. Thomas, R. M. Fulrath and R. M. Fisher (University of California Press, Berkeley, 1972) p. 1141.
20. S. C. DANFORTH and M. H. RICHMAN, *Metallogr.* **9** (1976) 321.
21. D. R. MESSIER and P. WONG, *J. Amer. Ceram. Soc.* **56** (1973) 480.
22. H. WADA, M. -J. WANG and T -Y. TIEN, *ibid.* **71** (1988) 837.
23. K. G. NICKEL, M. J. HOFFMANN, P. GREIL and G. PETZOW, *Adv. Ceram. Mater.* **3** (1988) 557.
24. S. M. BOYER and A. J. MOULSON, *J. Mater. Sci.* **13** (1978) 637.
25. C. O'MEARA, G. L. DUNLOP and R. POMPE, in "High Tech Ceramics", edited by P. Vincenzini, (Elsevier Science, Amsterdam, 1987) p. 265.

*Received 2 September 1991*
*and accepted 24 July 1992*